RESIDUAL SEISMIC PERFORMANCE OF AN EARTHQUAKE-DAMAGED RC INFILLED WALL

[1]Chien-Kuo Chiu, [2]Wen-I Liao, [2]Chu-Tsen Liao

Professor/Chairman, Department of Civil and Construction Engineering,
National Taiwan University of Science and Technology, Taipei, Taiwan

Department of Civil Engineering,
National Taipei University of Science

SUMMARY

In Taiwan, the reinforced concrete (RC) infill walls are often used for exterior and interior walls in general buildings. Due to the higher lateral stiffness and strength of the RC infill walls, it is necessary to understand the residual seismic capacity of RC infill walls damaged by an earthquake. To quantify the post-earthquake residual seismic capacity of RC infill wall members, experimental data for 6 wall specimens with shear failure are used to obtain the residual seismic capacity of damaged RC infill members for specified damage levels in this work. Different from the previous static loading test research, dynamic loading is also used to evaluate the residual seismic capacity of RC infill wall members. Besides the experiment data, the reduction factors of strength and stiffness for damaged RC infill wall members with and without horizontal interface slippage are also investigated, respectively. Finally, the modified method of the mechanical properties of RC infill walls corresponding to damage levels is proposed, and verified by using the strength development curve of the test data of damaged specimens. Restated, following the proposed seismic damage quantification method and mechanical properties of damaged RC infill walls, their residual seismic capacity can be considered in the pushover analysis.

Keywords*: RC infill wall, seismic damage quantification, interface slippage, dynamic loading, reduction factor, damage level.*

INTRODUCTION

After an earthquake, the overall structure or parts of a building suffer various degrees of damage, which must be quantitatively or qualitatively specified to evaluate the residual seismic capacity of the building to withstand further earthquakes. As part of the post-earthquake emergency assessment process [1-4], a rapid assessment of earthquake-damaged buildings must be performed to determine the safety of the damaged building and subsequent repair requirements. After emergency assessors have visually inspected structural damaged members, the residual seismic capacity of the damaged building can be obtained from the damage level of each member of a selected building. The main evaluation objects are vertical members (such as columns and walls). The JBDPA guidelines [2, 5] clearly specify the damage levels of vertical members in terms of the maximum residual crack width and concrete/rebar damage degree, as provided in Table 1.

In some studies, the reduction factors of seismic capacity that are associated with various damage levels have been experimentally investigated with the purpose of evaluating the residual seismic capacities of damaged RC column members after an earthquake. In Japan, the JBDPA guideline [5] suggests an energy dissipation capacity of a structural member for use in quantifying its residual seismic capacity following an earthquake and defines the reduction factor of energy dissipation as the ratio of the residual energy dissipation capacity to the original energy dissipation capacity. Maeda and Kang [6] proposed reduction factors of energy dissipation for structural members that corresponded to their damage levels, as shown in Table 2. The reduction factor is determined from the residual crack width and the overall damage state of the RC columns. The JBDPA guideline as revised in 2015 [2] also presents reduction factors of energy dissipation of various RC vertical members, as shown in Table 3.

Ito et al. [7] proposed reduction factors for the strength, deformation and damping ratio of damaged RC members for the purpose of assessing residual seismic capacity, based on experimental results for ten flexural members and seven shear members, as shown in Table 4. The damage levels and reduction factors of strength were determined from the background curve of each selected specimen. Ito et al. [7] calculated the reduction factors of deformation using the Park & Ang [8] damage index, which determines the degree of damage from the relationship between the limiting deformation and the energy. The reduction factors of the damping ratio were calculated from the hysteresis energy associated with the equivalent viscous damping ratio. In their post-earthquake seismic assessment, Ito et al. [7] obtained an accurate residual seismic capacity ratio of the structure, considering the reduction factors of the strength, deformation and damping ratio of the flexural and shear members of a building.

In most relevant studies, the designs of specimens differ from those of traditional low-rise buildings in Taiwan, and the reduction factors are obtained from limited test data. If the reduction factors must be applied to the current method of seismic performance assessment, then more reliable test data are required to obtain those. In addition, the practical application of these reduction factors to evaluate the seismic capacity of damaged buildings has rarely been investigated. Accordingly, Chiu et al. [9] used 40 sets of test data for column members that conform to Taiwan's traditional low-rise building design to obtain the reduction factors of the strength, stiffness and energy dissipation of damaged RC column members with various failure modes. These reduction factors for RC column members were used to modify the nonlinear plastic hinges in nonlinear pushover analysis, and an actual post-earthquake damaged RC building was considered to demonstrate the proposed detailed seismic performance assessment. However, Chiu et al. [9] obtained the reduction factors of only damaged RC column members to provide a detailed seismic performance assessment of a damaged RC building structure. Since other kinds of vertical member also affect the residual seismic capacity of a damaged RC building, their residual seismic capacity, which is related to damage level, should be further studied, especially for RC infill walls. Generally, although an RC infill wall is regarded as a non-structural member in building design, its seismic resistance cannot be neglected in seismic performance assessment.

In typical low-rise RC buildings in Taiwan, RC infill walls are commonly used to divide rooms and households, providing personal privacy. These walls are generally designed to meet the minimal requirement of reinforcement in ACI 318-14 [10]. Like RC column and shear wall members, RC infill walls can contribute to strength and stiffness during an earthquake. Therefore, before or after an earthquake, the residual seismic capacity of RC infill walls should be considered in the seismic performance assessment of a typical low-rise RC building. Moreover, for a damaged RC infill wall, its damage level and its residual seismic capacity cannot easily be determined. Therefore, the main purpose of this work is to propose a seismic damage quantification method and mechanical properties of seismic capacity for a damaged RC infill wall.

This work, like that of Chiu et al. [9], focuses on the residual seismic capacity of RC infill walls in Taiwan's traditional low-rise street houses. To obtain the residual seismic capacity of damaged RC infill wall members, two series of RC infill wall specimens (C25W15 and NEW-C25W15) are designed and used. In addition to the ordinary static loading test, a dynamic loading test is performed to evaluate the residual seismic capacity of RC infill wall members including the reduction factors of strength and stiffness. Finally, a model that can be used to determine the mechanical properties of an RC infill wall with a specified damage level is proposed.

Table 1 Classification criteria for each damage level of structural members in JBDPA [2, 5]

Damage level	Description of damage (Visual inspection state)		
	Residual crack widths, w	Concrete	Rebars
I (Slight)	w< 0.2 mm.	Narrow cracks on concrete surface	-
II (Light)	0.2<w<1 mm	Visible cracks on concrete surface	-
III (Moderate)	1<w<2 mm.	Localized crushing of concrete cover	-
IV (Severe)	w>2 mm.	Spalling off of cover concrete.	Crushing of concrete with exposed reinforcing bars.
V (Collapse)	-	Crushing of core concrete	Buckling of reinforcing bars.

Table 2 Reduction factors of energy dissipation of different members [6]

Damage level	Ductile column	Brittle column and Shear wall
I	0.95	0.95
II	0.75	0.6
III	0.5	0.3
IV	0.1	0
V	0	0

Table 3 Reduction factors of energy dissipation of different RC members [2]

Damage Level	RC column			RC wall		RC beam	
	Shear	Flexural -shear	Flexural	Shear	Flexural	Shear	Flexural
I	0.95	0.95	0.95	0.95	0.95	0.95	0.95
II	0.6	0.7	0.75	0.6	0.7	0.7	0.75
III	0.3	0.4	0.5	0.3	0.4	0.4	0.5
IV	0	0.1	0.2	0	0.1	0.1	0.2
V	0	0	0	0	0	0	0

Table 4 Reduction factors of strength η_V, deformation η_d and damping ratio η_h [7]

Damage Level	Flexural member			Shear member		
	η_V	η_d	η_h	η_V	η_d	η_h
I	1	1	0.95	1	1	0.9
II	1	0.95	0.8	1	0.85	0.7
III	1	0.85	0.75	1	0.75	0.6
IV	0.6	0.75	0.7	0.4	0.7	0.5
V	0	0	0	0	0	0

Experimental program and test results

To investigate the residual seismic capacities of RC infill wall members, six 1/2-scale RC infill wall specimens (clear height/width = 0.67) are statically and dynamically loaded. In Fig. 1, each specimen comprises four parts, which are columns, web, top beam, and foundation. The columns of each specimen are 150 cm long and their cross-sections are 25 cm × 25 cm. The main bars are SD420W of D16, and the stirrups are SD280W of D10 with a spacing of 20 cm (Table 5_a). The width and thickness of each wall web in each specimen are 225 cm and 15 cm, respectively. These specimens are divided into the C25W15 and NEW-C25W15 series. The C25W15 series was the original design of RC infill wall, and the slippage was observed at the interface between the wall web and the foundation during the test. In order to investigate the difference between the RC infill walls with or without horizontal interface slippage, the NEW-C25W15 series used the same design as the C25W15 series but with a higher longitudinal reinforcement ratio.

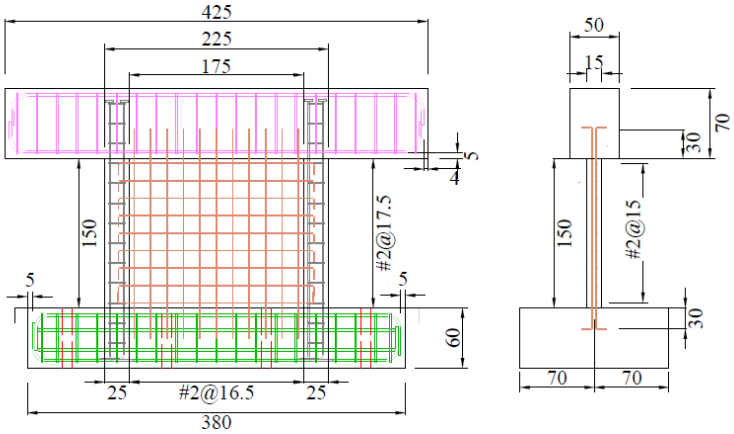

Fig. 1 Detailed reinforcement arrangement of the C25W15 series specimen

For the C25W15 series, the longitudinal and transverse reinforcements are SD420W of D7, and their reinforcement ratios are 0.264 % and 0.241 %, respectively. For the NEW-C25W15 series, the longitudinal and transverse reinforcements are SD420W of D10, and their reinforcement ratios are 0.597 % and 0.570 %, respectively. The cross-sections of the top beam and foundation are 50 × 70 cm and 140 × 60 cm, and the lengths are 425 cm and 380 cm, respectively. The main bars of both the top beam and the foundation are SD420W of D25, and the stirrups are SD280W of D13 with a spacing of 20 cm. The actual compressive strength of each part of concrete is 22.7 – 39.5 MPa. Table 5(b) presents detailed design information for each specimen.

This experimental system herein uses two lateral actuators to provide lateral forces in the in-plane direction; two vertical actuators to simulate the horizontal movements of floors, pulleys, and side stays, which were installed in the out-of-plane direction to simulate the unidirectional lateral thrust; and two oil jacks that provide an axial loading of $0.1A_g f_c'$. Using an optical measurement system, 64 markers are placed on each specimen to measure the deformation during the test. Displacement gauges are set on the upper and lower parts of each specimen to measure the displacement of the foundation. To quantify damage, crack widths are measured using a microscope with a

resolution of 0.01 mm. Along with the maximum crack width at a specified peak deformation, the corresponding residual crack width under an applied loading of zero is recorded. In the static-cyclic loading stage, when a specimen is seriously damaged or the applied force is reduced to 60 % of its maximum strength, the test is stopped.

Table 5(a) Material properties of deformed bars

			Mechanical Properties			
	Division	Symbol	Yield point (N/mm^2)	Tensile (N/mm2)	Percentage of elongation (%)	Bend angle
CNS 560 A2006	Deformed bars	SD420W	420~540	550 above	12 above	180◦
		SD280W	280~380	420 above	14 above	180◦
		Diameter of bar				
		D7	D10	D13	D16	D25
		7mm	10mm	13mm	16mm	25mm

Table 5(b) Material properties of specimens

Specimen	C25W15-S	C25W15-II	C25W15-III	C25W15-IV	NEW-C25W15-S	NEW-C25W15-III
Compressive strength (MPa)	36.6	35.0	38.6	39.5	22.7	23.2
Clear height (cm)	150	150	150	150	150	150
Width (cm)	225	225	225	225	225	225
Thickness (cm)	15	15	15	15	15	15
Longitudinal reinforcement ratio of web(%)	0.264	0.264	0.264	0.264	0.597	0.597
Transverse reinforcement ratio of web (%)	0.241	0.241	0.241	0.241	0.570	0.570
Cross section of boundary column	25 × 25	25 × 25	25 × 25	25 × 25	25 × 25	25 × 25
Main bar of boundary column	6-SD420W #5	6-SD420W #5	6-SD420W #5	6-SD420W #5	6-SD420W #5	6-SD420W #5
Stirrup of boundary column	SD280W #3@20 cm	SD280W #3@20 cm	SD280W #3@20 cm	SD280W #3@20 cm	SD280W #3@20 cm	SD280W #3@20 cm

In this work, dynamic loading is used to damage a specimen to a specified level and then static-cyclic loading is used to investigate its residual seismic capacity [21]. Since each specimen is dynamically loaded with displacement control in the experiment, the displacement history of each specimen is obtained from a non-linear analysis of a traditional low-rise street house in Taiwan. Therefore, the designed specimens are assumed to be the RC infill wall members in a selected building structure. The selected building structure has five floors with a horizontal span (four spans in total) of 17.28 m and a longitudinal span (three spans in total) of 11.5 m. The first floor is 3.45 m high, and the other floors are 3 m high. The slab thickness of each floor is 12 cm. The targeted building is on the one category (hard) site in Yujing Dist., Tainan City. Consistent with the seismic design specifications for buildings in Taiwan, the seismic demand of the building is given by S_{DS} = 0.7 and S_{D1} = 0.4, and the peak ground acceleration A_T is 0.28 g, which corresponds to a design earthquake with a returning period of 475 years.

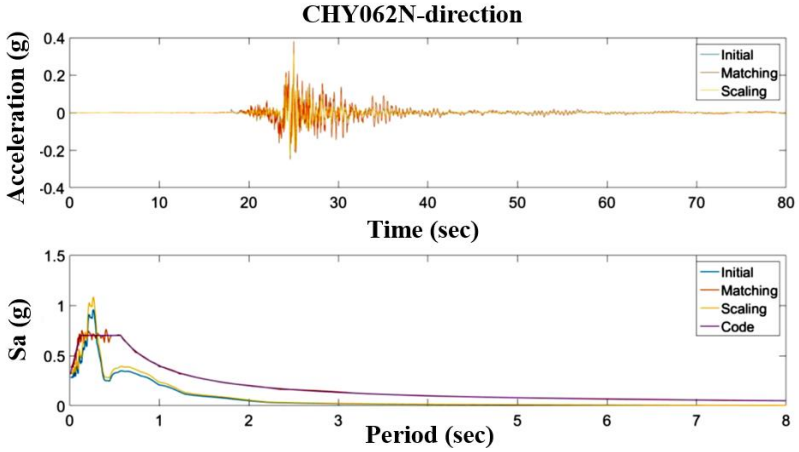

Fig. 2 Artificial seismic history and response spectrum

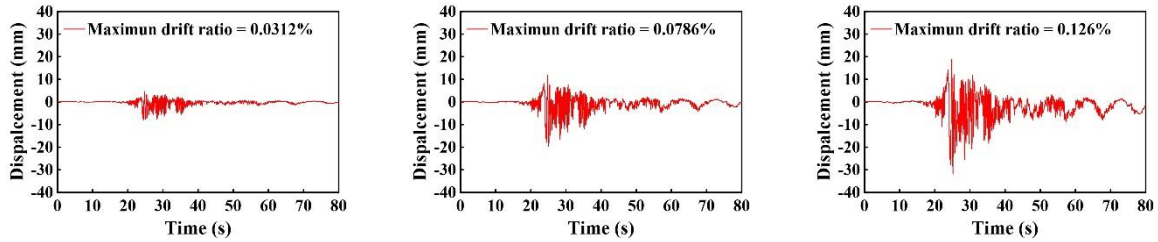

(a) Damage level II (b) Damage level III (c) Damage level IV

Fig. 3 The displacement histories of the dynamic loading

To provide the time history of an earthquake, which is required in structural dynamic analysis, the original acceleration time-history of the location of building CHY062 [22] during the Meinong Earthquake on February 6, 2016, is used. The time-history data are converted into an artificial earthquake, compatible with the design response spectrum that is required by the relevant code in Taiwan, as shown in Fig. 2, for use in nonlinear time-history analysis. Ucar et al. [23] proposed a modified energy-balance equation accounting for P-delta effects and hysteretic behavior of reinforced concrete members. Both of pushover analysis and nonlinear time history analysis of several RC frames having different numbers of stories is performed using the structural analysis program SAP2000 (2016), and the nonlinear modeling or nonlinear time-history analyses of the selected RC building are also described. In this work, the nonlinear time-history analysis of selected building is performed by ETABS, and the foundation of the 3D structural model is assumed to be the fixed end. Additionally, the slab with a live load of 200 kgf/cm^2, is modeled using the shell element and assumed to be the rigid diaphragm. The P-delta effect in each member is not considered, and flexural and shear plastic hinges defined by the NCREE [24] are set up on beam and column members, respectively. Furthermore, the hysteretic behavior of a beam/column member is modeled by the Takeda model [25] Based on the structural dynamic analysis, one of the RC infill wall members in the first floor with an axial force of approximately $0.1A_g f_c^{'}$ is used to determine the dynamic loading of a specimen. In order to make a wall specimen reach a specified degree of damage in the dynamic experiment, the time histories of displacement data are obtained by adjusting the intensity of the input earthquake from the nonlinear dynamic analysis. The time histories of displacement data are used to be the control signals of the dynamic actuator of each specimen (Fig. 3). The experimental results for specimens C25W15-S and NEW-C25W15-S are used to determine the corresponding intensity of an earthquake for each specimen, based on nonlinear time-history analysis. Table 6 provides the loading scheme for each specimen in both the dynamic test and the static-cyclic loading test (loading protocol in Fig. 4 [26]).

Test results

Fig. 5 plots the input displacement signals that are obtained by structural dynamic analysis and output displacement signals measured by displacement gauges that are installed in the top of a specimen. Fig. 5 indicates that the maximum errors between input and output of different damage levels are 5.1 mm, 6.9 mm and 11.1mm, respectively. The main reason related to the difference between the input and out displacement signals during the dynamic loading test, as shown in Fig. 5 could be attributed to the high stiffness of the wall specimens. In this work, after a specimen is damaged to a specified level by dynamic loading, static-cyclic loading is applied to determine the residual seismic capacity. Since one or more loading cycles have been applied on a specimen during the dynamic loading, the specimen is damaged after the loading. Therefore, the initial stiffness obtained during the

dynamic loading is higher than that obtained during the static-cyclic loading. Fig. 6 plots the relationship between the lateral force and the deformation of each specimen in the experiment under both dynamic and static-cyclic loadings.

Reduction factors of mechanical properties

(1) Reduction factor of strength

Fig. 7 presents the difference in strength degradation of specimens that are damaged under dynamic loading and static-cyclic loading. The reduction factor of strength is defined as V/V_{max} (where V_{max} is the maximum lateral force during testing) and plotted on the Y-axis in Fig. 7, based on the experimental results. Before the maximum lateral force is reached, the reduction factor of strength is set to 1.0. From the figure, the reduction factors of strength of the specimens that are damaged by dynamic are close to those damaged by static-cyclic loadings. Based on Fig. 7, the strength reduction factors did not decline before drift ratio of 0.8 % was reached. When the drift ratio reached 1 % (damage level III), the strength reduction factor significantly declined. The NEW-C25W15 series of specimens exhibited a much greater reduction of strength than the C25W15 series of specimens with horizontal interface slippage.

Table 6 Loading schemes of each specimen

Specimen	Dynamic loading protocol Maximum drift ratio (%) Input / Output	Static-cyclic loading protocol Maximum drift ratio (%), 2 cycles
C25W15-S	-	±0.03125 %、±0.0625 %、±0.125 %、±0.25 %、±0.375 %、±0.5 %、±0.75 %、±1.0 %、±1.5 %、±2.0 %
C25W15-II	0.52 % / 0.18 %	±0.25 %、±0.375 %、±0.5 %、±0.75 %、±1.0 %、±1.5 %、±2.0 %
C25W15-III	1.31 % / 0.85 %	±1.0 %、±1.5 %、±2.0 %
C25W15-IV	2.12 % / 1.38 %	±1.5 %、±2.0 %
NEW-C25W15-S	-	±0.03125 %、±0.0625 %、±0.125 %、±0.25 %、±0.375 %、±0.5 %、±0.75 %、±1.0 %、±1.5 %、±2.0 %
NEW-C25W15-III	0.52 % / 0.18 %	±0.25 %、±0.375 %、±0.5 %、±0.75 %、±1.0 %、±1.5 %、±2.0 %

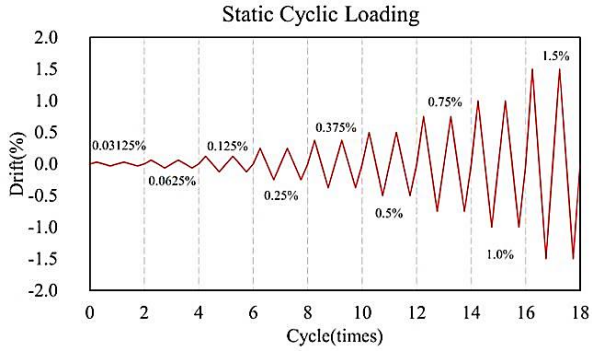

(a) Static-cyclic loading protocol [26]

(b) Location of displacement gauges

Fig. 4 Static-cyclic loading protocol and location of displacement gauges

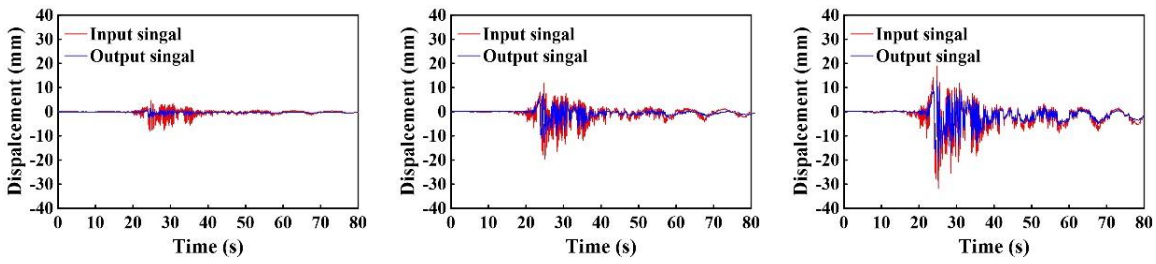

(a) Damage level II (b) Damage level III (c) Damage level IV

Fig. 5 The comparison of input and output signals of the displacement histories

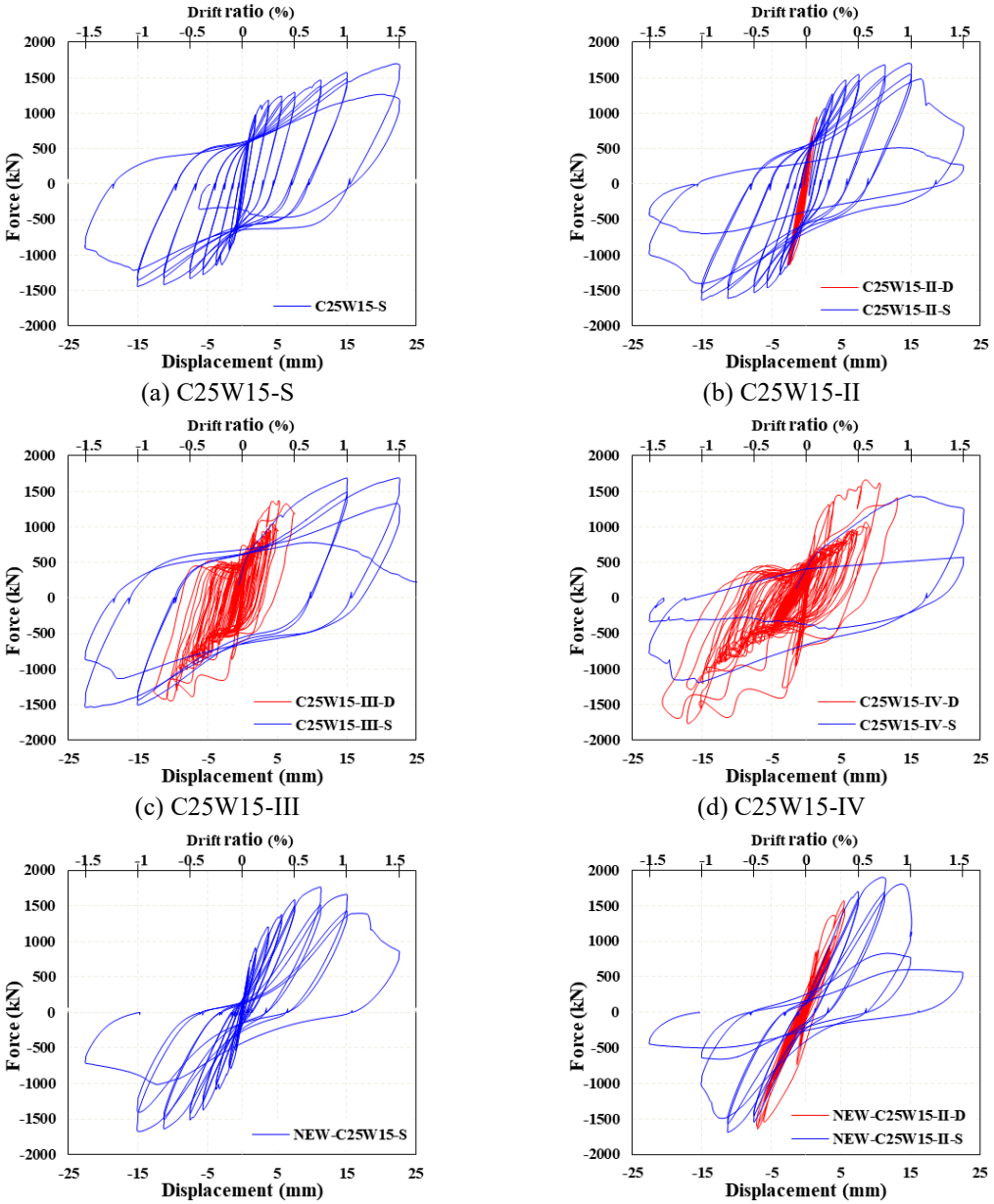

(a) C25W15-S (b) C25W15-II

(c) C25W15-III (d) C25W15-IV

(e) NEW-C25W15-S (f) NEW-C25W15- III

Fig. 6 Relationship of the lateral force and deformation of each specimen

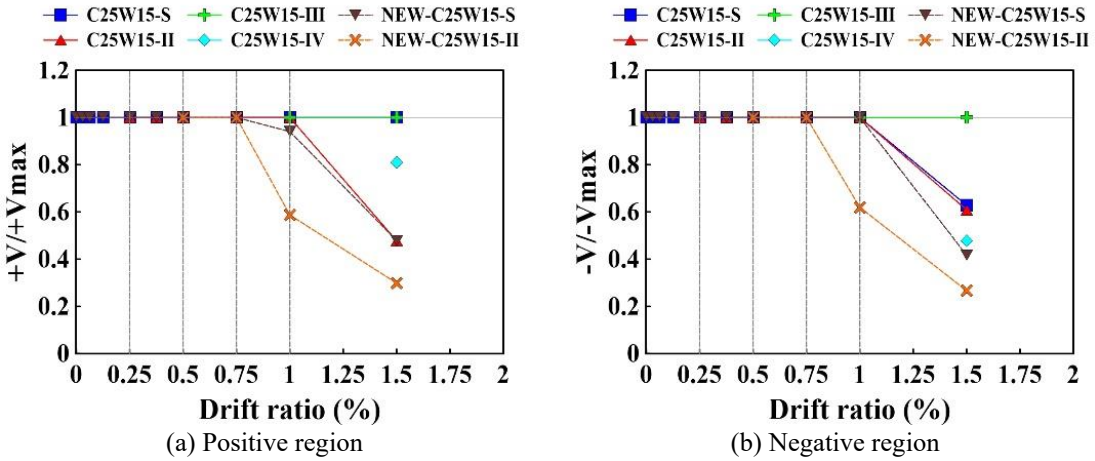

(a) Positive region (b) Negative region

Fig. 7 Relationship curves between the deformation and reduction factor of strength for the selected specimens

Based on the dividing points of deformation between damage levels and Fig. 7, the reduction factors of strength at each damage level are determined. Based on Fig. 19, the strength of specimens at damage levels I, II and III is assumed not to decrease and the reduction factors of strength at damage levels I, II and III are set to 1.0. The reduction factors at damage level IV are obtained as the average reduction factor of all specimens at a deformation of 1.5 % (ultimate deformation point). Table 13 lists the suggested reduction factors of strength η_V at each damage level for an RC infill wall member with or without interface slip. The damage state of the specimen with shear failure is used to determine its damage level. Since the maximum lateral force is at the dividing point between damage levels III and IV, the strength declines greatly in damage levels IV and V. The residual strength in damage levels IV and V is assumed to be zero.

(2) Reduction factor of stiffness

Fig. 8(a) plots the relationship between the deformation and reduction factor of stiffness, which is the ratio of the equivalent stiffness to the yielding stiffness. The equivalent stiffness is defined as the slope of a line that connects the positive and negative points of the force-displacement curve at a specified deformation [27], as shown in Fig. 8(b). From Fig. 8(a), for all specimens, the reduction factors of stiffness decrease as the deformation increases, following an almost exponential curve. The reduction factors that are obtained from the specimens that are damaged by dynamic loading are similar to those obtained from specimens that are damaged by static-cyclic loading. The reduction factors that are obtained from the specimens with interface slip are slightly lower than those obtained from the specimens without interface slip.

Based on the dividing points of deformation between damage levels and Fig. 8(a), the average reduction factor of stiffness at each damage level is determined from each specimen. Table 7 lists the experimental reduction factors of stiffness η_k at various damage levels. Clearly, at damage level I (drift ratio of 0.25%), since the specimens have cracked, the stiffness values are reduced to 0.4. Additionally, the reduction factors at damage level IV are calculated from the dividing point between damage levels IV and V, which is ultimate deformation point.

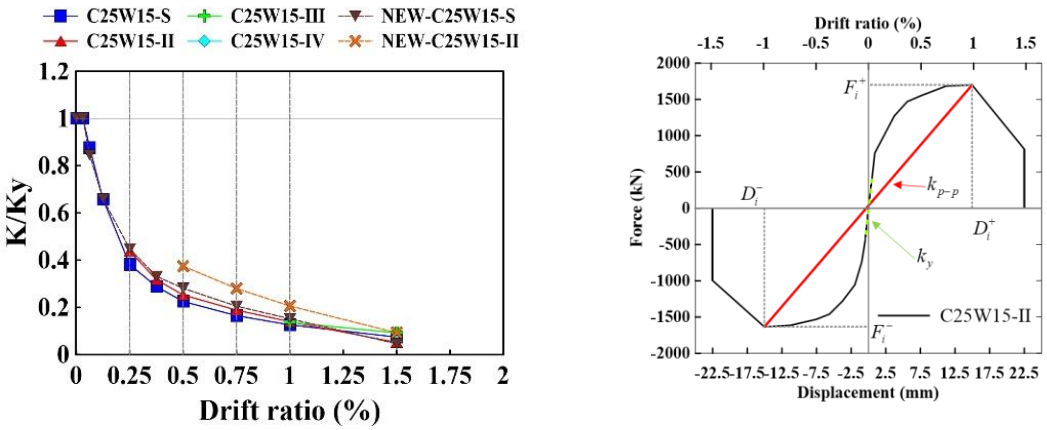

(a) Stiffness reduction (b) Equivalent stiffness [27]

Fig. 8 Relationship curves between the deformation and reduction factor of stiffness (equivalent stiffness) for the selected specimens

Table 7 Reduction factors of strength and stiffness of RC infill wall members for each damage level

Damage level	With interface slip			Without interface slip		
	η_v	η_k	η_E	η_v	η_k	η_E
I	1	0.4	0.95	1	0.4	0.95
II	1	0.25	0.85	1	0.35	0.9
III	1	0.1	0.55	1	0.25	0.75
IV	0 (0.6)	0 (0.07)	0(0.1)	0 (0.4)	0 (0.1)	0(0.4)
V	0	0	0	0	0	0

Note： The value in the parentheses represent experimental deformations.

(3) Reduction factor of energy dissipation

The reduction factor of energy dissipation η_E, which is defined as the ratio of the residual energy dissipation capacity to the original energy dissipation capacity [2] is calculated from the experimentally obtained envelope curve. Fig. 9 plots the relationship between the deformation and reduction factor of energy dissipation. Based on Fig. 9, for all specimens, the reduction factors of energy dissipation decrease as the deformation increases, following an almost straight line beyond a drift ratio of 0.2 %. Additionally, the reduction factors that are obtained from specimens that are damaged by dynamic loading are slightly lower than those obtained from specimens that

are damaged by static-cyclic loading. The reduction factors that are obtained from the specimens with interface slip are slightly lower than those obtained from the specimens without the horizontal interface slippage.

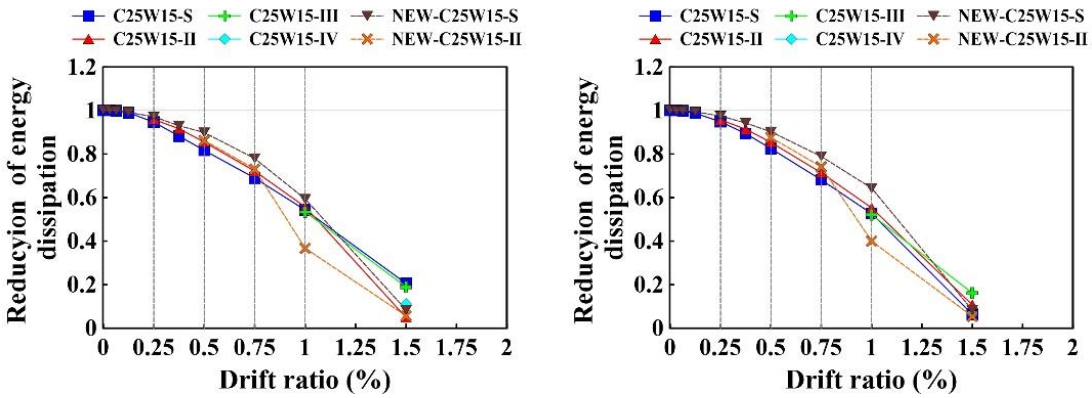

(a) Positive region (b) Negative region

Fig. 9 Relationship curves between the deformation and reduction factor of energy dissipation for the selected specimens

Based on the definition of residual mechanical properties, Table 7 lists the reduction factors of strength, stiffness and energy dissipation for RC infill wall members with and without horizontal interface slippage. Generally, since an RC infill wall is a member with high stiffness brittle failure and low ductility, its reduction factor of energy dissipation is not considered. Experimental results for RC infill wall specimens reveal that their strength declines significantly after the maximum strength point is reached. Therefore, the residual strength at damage levels IV and V is assumed to be zero, as shown in Table 7.

Conclusions

For the damage quantification for an RC infill wall member in the practical use, this work concluded the damage pattern and limiting deformation for each damage level. Restated, an engineer can follow the proposed criteria to determine the damage level of a damaged RC infill wall after an earthquake. On the base of the experimental data, this work provided reduction factors of seismic capacity for RC infill walls with shear failure modes. Additionally, for damaged RC infill wall members with and without the interface slip, the residual strength and residual stiffness can be quantified using the suggested reduction factors summarized in Table 7. For the seismic assessment of a damaged low-rise RC building with RC infill walls, this work proposed a method that can be used to define the mechanical properties for damaged RC infill wall members corresponding to their damage levels. Furthermore, the detailed SST model and simplified SST model were suggested to the maximum shear strengths for RC infill wall members with and without horizontal interface slippage, respectively. However, this work adopted the experimental results to identify the deformation induced by the horizontal interface slippage. In the future, the theoretical model should be development to quantify the horizontal interface slippage of an RC infill wall member under an earthquake.

Reference

[1] ATC, Applied Technology Council (1989). “Procedures for post-earthquake safety evaluation of buildings.” ATC-20, Redwood City, CA.

[2] JBDPA (Japan Building Disaster Prevention Association, 2015). “Standard for seismic evaluation of existing reinforced concrete buildings, guidelines for seismic retrofit of existing reinforced concrete buildings, and technical manual for seismic evaluation and seismic retrofit of existing reinforced concrete buildings.” Tokyo, Japan.

[3] New Zealand Society for Earthquake Engineering (2014). “Field Guide: Rapid Post Disaster Building Usability Assessment-Earthquakes.” New Zealand.

[4] CPAMI, The Rapid-assessment Regulations for Disaster-damaging Buildings, Construction and Planning Agency Ministry of the Interior, 2009, Taiwan. https://www.cpami.gov.tw.

[5] JBDPA (Japan Building Disaster Prevention Association, 2001). Guideline for Post-earthquake Damage Evaluation and Rehabilitation of RC buildings, Tokyo, Japan. (in Japanese)

[6] Maeda Ma., Kang D. E., (2014). “Post Earthquake Damage Evaluation of Reinforced Concrete Buildings.” Journal of Advanced Concrete Technology, 7(3), 327-335. https://doi.org/10.3151/jact.7.327

[7] Ito Y., Suzuki Y., Maeda M., (2015). “Residual Seismic Performance Assessment for Damaged RC Building Considering the Reduction of Strength, Deformation and Damping Ratio.” Proceeding of JCI Annual Convention (Japan Concrete Institute), 37(2), 787-792.

[8] Park Y.J., Ang A. H-S., (1985). “Mechanistic Seismic Damage Model for Reinforced Concrete.” Journal of the Structural Engineering, 111(4): 722-739. https://doi.org/10.1061/(asce)0733-9445(1985)111:4(722)

[9] Chiu, C. K., Sung, H. F., Chiou. T .C. (2021) " Quantification of the reduction factors of seismic capacity for damaged

RC column members using the experiment database." Earthquake Engineering & Structural Dynamics, 50(3), 756-776. https://doi.org/10.1002/eqe.3355
[10] ACI Committee 318. (2014). "Building code requirements for structural concrete (ACI 318-14) and commentary (ACI 318R-14)." ACI Committee 318, Farmington Hills, MI
[11] ACI Committee 318 (2019) "Building Code Requirements for Structural Concrete (ACI 318-19) and Commentary (ACI 318R-19)," American Concrete Institute (ACI), Farmington Hills, Mich.
[12] Hwang, S. J., and Lee, H. J. (2002). "Strength prediction for discontinuity regions by softened strut-and-tie model." Journal of Structural Engineering, 130(3), 529-530. https://doi.org/10.1061/(asce)0733-9445(2002)128:12(1519)
[13] Tsai, R. J. (2015). "Prediction of lateral load displacement curves of reinforced concrete wall with openings." M.S. thesis, Department. of Civil Engineering, National Taiwan University, Taipei, Taiwan (in Chinese).
[14] Hwang, S. J., Tsai, R. J., Lam, W. K., and Moehle, J. P. (2017). "Simplification of softened strut-and-tie model for strength prediction of discontinuity regions." ACI Structural Journal, 114(5). https://doi.org/10.14359/51689787
[15] Zhang, L. X. B. and Hsu, T. T. C. (1998). "Behavior and Analysis of 100 MPa Concrete Membrane Elements." Journal of Structural Engineering, ASCE, 124(1), 24-34. https://doi.org/10.1061/(asce)0733-9445(1998)124:1(24)
[16] Vecchio, F. and Collins, M. (1993). "Compression Response of Cracked Reinforced Concrete." Journal of Structural Engineering.", 119(12), 3590-3610. https://doi.org/10.1061/(asce)0733-9445(1993)119:12(3590)
[17] Hwang, S. J., Fang, W. H., Lee, H. J., and Yu, H. W. (2001). "Analytical Model for Predicting Shear Strength of Squat Walls." Journal of Structural Engineering, 127(1), 43-50. https://doi.org/10.1061/(asce)0733-9445(2001)127:1(43)
[18] Oesterle, R. G., Aristizabal, J. D., Shiu, K. N., and Corley, W.G. (1984). "Web Crushing of Reinforced Concrete Structural Walls." ACI Journal Proceedings, 81(3), 231-241. https://doi.org/10.14359/10679
[19] Tu Y. S. (2005) "An Analytical Study of the Lateral Load-Deflection Responses of Low Rise RC Walls and Frames." Ph.D. thesis Department of Civil and Construction Engineering, National Taiwan University of Science and Technology, Taipei, Taiwan (in Chinese).
[20] NZS3101, Concrete Structures Standard, The design of Concrete Structures & Commentary on the Design of Concrete Structures, New Zealand Standard, 2006.
[21] Marder, K. J., Motter, C. J., Elwood KJ, Clifton GC. (2018). "Effects of variation in loading protocol on the strength and deformation capacity of ductile reinforced concrete beams." Earthquake Engineering and Structural Dynamics, 47(11), 2195-2213. https://doi.org/10.1002/eqe.3064
[22] ASCII (1999). Original seismic data of Taiwan Chi-Chi earthquake. Available at https://scweb.cwb.gov.tw/special/19990921pga.asp.
[23] Ucar, T., Merter, O. (2018), "Derivation of energy-based base shear force coefficient considering hysteretic behavior and P-delta effects", Earthquake Engineering and Engineering Vibration, 17(1), 149-163.
[24] NCREE (2013), Technology handbook for seismic evaluation and retrofit of school buildings (NCREE-13-023), National Center for Research on Earthquake Engineering of Taiwan, Taipei, Taiwan. (in Chinese).
[25] Takeda, T., M. A. Sozen and N. N. Nielsen (1970) "Reinforced Concrete Response to Simulated Earthquakes," Journal, Structural Division, ASCE, 96(ST12), 2557-2573.
[26] ACI Committee 374 (2013). "Guide for Testing Reinforced Concrete Structural Elements under Slowly Applied Simulated Seismic Loads (ACI374.2R-13)." American Concrete Institute, 1-18.
[27] Di Ludovico M, Polese M, d'Aragona MG, Prota A, Manfredi G. "Aproposal for plastic hinges modification factors for damaged RC columns. " Engineering Structures. 2013;51, 99–112. https://doi.org/10.1016/j.engstruct.2013.01.009